



**HAL**  
open science

## X-ray microtomography studies of localised corrosion and transitions to stress corrosion cracking

B.J. Connolly, D. Horner, S.J. Fox, A.J. Davenport, C. Padovani, S. Zhou, A. Turnbull, M. Preuss, N.P. Stevens, T.J Marrow, et al.

► **To cite this version:**

B.J. Connolly, D. Horner, S.J. Fox, A.J. Davenport, C. Padovani, et al.. X-ray microtomography studies of localised corrosion and transitions to stress corrosion cracking. *Materials Science and Technology*, 2006, 22 (9), pp.1076-1085. 10.1179/174328406X114199 . hal-00436212

**HAL Id: hal-00436212**

**<https://hal.science/hal-00436212>**

Submitted on 17 May 2023

**HAL** is a multi-disciplinary open access archive for the deposit and dissemination of scientific research documents, whether they are published or not. The documents may come from teaching and research institutions in France or abroad, or from public or private research centers.

L'archive ouverte pluridisciplinaire **HAL**, est destinée au dépôt et à la diffusion de documents scientifiques de niveau recherche, publiés ou non, émanant des établissements d'enseignement et de recherche français ou étrangers, des laboratoires publics ou privés.



Distributed under a Creative Commons Attribution - NonCommercial 4.0 International License

# X-ray microtomography studies of localised corrosion and transitions to stress corrosion cracking

B. J. Connolly\*<sup>1</sup>, D. A. Horner<sup>1</sup>, S. J. Fox<sup>1</sup>, A. J. Davenport<sup>1</sup>, C. Padovani<sup>1</sup>, S. Zhou<sup>2</sup>, A. Turnbull<sup>2</sup>, M. Preuss<sup>3</sup>, N. P. Stevens<sup>3</sup>, T. J. Marrow<sup>3</sup>, J.-Y. Buffiere<sup>4</sup>, E. Boller<sup>5</sup>, A. Groso<sup>6</sup> and M. Stampanoni<sup>6</sup>

Two forms of high resolution X-ray tomographic experiments (i.e. synchrotron based X-ray microtomography and desktop microfocus computed X-ray tomography) are demonstrated in the present paper to illustrate the wide application of these techniques for qualitative and quantitative studies of localised corrosion and environmentally assisted cracking. Specifically, synchrotron based X-ray tomography was used to investigate the localised corrosion morphology within aluminium specimens when exposed in situ to a chloride environment while microfocus computed X-ray tomography was used to investigate the morphology and quantify the transition from localised corrosion to stress corrosion cracking in steel specimens exposed ex situ to a simulated corrosive condensate environment.

Keywords: Corrosion, Stress corrosion cracking, X-ray microtomography

## Introduction

X-ray tomography is a non-destructive technique that allows for three-dimensional (3D) observations and analysis of microstructure, defects and damage in the interior of opaque materials with resolution on the micrometre scale.<sup>1-4</sup> The medical profession has been using computed tomography (e.g. CT scanners, CAT scans) to produce non-invasive, cross-sectional images of bone and tissue since the early 1970s, albeit with typical resolution capability of 300–1000  $\mu\text{m}$ .<sup>3,4</sup> Full use of the potential of this technique by materials scientists who often require much greater spatial as well as temporal resolution in their studies has been limited until recent years. Spatial resolutions better than 10  $\mu\text{m}$  have only recently been achieved in the late 1980s.<sup>5</sup> Development of third generation synchrotron facilities has made it possible to achieve micrometre to submicrometre resolutions, making the technique increasingly desirable for materials characterisation studies.<sup>4</sup>

Visualisation in synchrotron X-ray tomography is based on the variations in absorption coefficients of the material along the path of the transmitted X-ray beam through a specimen. The absorption coefficient is linked

to the density and atomic number of the different materials within an object making visualisation of defects or second phase particles versus the bulk material easily determined. 3D maps of the variation in absorption coefficient are generated by acquiring multiple two-dimensional (2D) radiographs (i.e. a superimposed volume of attenuation information on a 2D plane) while rotating a sample between 0 and 180°. When the angular step is small, the local absorption coefficient in 3D space is computed using a filtered back project algorithm resulting in contrasts between different materials within the specimen.

Recently laboratory based instruments with resolutions on the order of 5–10  $\mu\text{m}$  have also been developed. Desktop tomographic instruments<sup>6,7</sup> with a microfocus X-ray tube provide a viable alternative for the high quality microtomography at synchrotron sources. These systems operate based on the same principles as that of synchrotron based instruments but offer advantages such as small footprint, ease of operation and access. Disadvantages include longer scan times, 1000 times smaller flux capacity and limited maximum resolution owing to the size of the microfocus spot size.<sup>4</sup> Care also must be taken as microfocus X-ray sources use a polychromatic beam compared with a monochromatic beam in a synchrotron source. Reconstructions from data obtained from a polychromatic X-ray may result in beam hardening artefacts.<sup>4</sup> Beam hardening artefacts can be mitigated with the use of a filter which is intended to preharden the spectrum.<sup>8</sup> Regardless, quantitative reconstruction of the absorption coefficients should not be conducted without calibration.<sup>4</sup>

<sup>1</sup>Metallurgy and Materials, University of Birmingham, Edgbaston, Birmingham, UK

<sup>2</sup>Materials Centre, National Physical Laboratory, Teddington, Middlesex, UK

<sup>3</sup>School of Materials, The University of Manchester, Manchester, UK

<sup>4</sup>GEMPPM INSA, Lyon, France

<sup>5</sup>European Synchrotron Radiation Facility, Grenoble, France

<sup>6</sup>Swiss Light Source, Paul Scherrer Institute, Villigen, Switzerland

\*Corresponding author, email b.j.connolly@bham.ac.uk

Over the past five to ten years microtomography has become an increasingly accepted and used technique to characterise 3D internal structures of material both in a qualitative and quantitative manner. In general, the majority of experiments have been performed on samples under static, *ex situ* conditions and have focused on either microstructural or damage/defect analysis. *Ex situ* conditions simply indicate that an action, whether it is a processing step or deformation, for example, is taken on the material of interest before X-ray exposure via the tomography technique. Examples of these types of tomographic experiments are extremely varied and include such studies as characterisation of the microstructure of ceramic filters<sup>9</sup> and metallic foams,<sup>2,4,10</sup> analysis of inclusions in rough diamonds,<sup>6</sup> 3D visualisation of grain structure and associated cracking of aluminium alloys,<sup>11,12</sup> and investigations of the effect of radiolytic and thermal oxidation on microstructure evolution in graphite.<sup>13,14</sup>

While *ex situ* X-ray tomography experiments will provide considerable information that is not otherwise readily collected, the most challenging and most rewarding use of this technique is through *in situ* investigation. Although one of the fundamental requirements of X-ray tomography is that the microstructure of the material should not change significantly during the scan, *in situ* visualisation has been performed under specific conditions. To date, *in situ* tomographic experiments have been conducted in conjunction with either a furnace, a loading stage and/or a corrosive aqueous environment. The first *in situ* experiments performed using a synchrotron source involved investigations of the initiation and damage within an aluminium metal matrix composite during tensile testing.<sup>15</sup> Quantitative results from the study indicated that although, qualitatively, the damage mechanism observed on the surface and within the specimen appeared similar, the damage growth rate was much higher within the specimen owing to different stress states associated with differing geometrical characteristics of particles as a function of position within the volume. These observations would not have been possible without use of X-ray tomography. The first truly *in situ* work was actually performed utilising a microfocus X-ray apparatus and a pneumatic loading device to assess the fatigue crack closure of an Al-Li alloy.<sup>16-18</sup> Results revealed mixed mode contact of the crack faces during the load cycle that would not have been observed by conventional methods. Further *in situ* work on fatigue nucleation<sup>11,19,20</sup> and closure<sup>17,21-23</sup> utilising a synchrotron source has produced additional insight into the controlling mechanism of fatigue crack behaviour. Other examples of *in situ* experiments using a loading stage include quantitative image analysis of nickel<sup>24</sup> and polyurethane<sup>25</sup> foams under tension and compression, and further analysis and modelling of damage initiation and growth in metal matrix composites.<sup>26-28</sup> Recently, with the development of an ultra fast X-ray tomographic set-up, experiments have been performed on systems that evolve on the time scale of a few seconds. Through the use of this equipment the evolution of the morphology associated with solidification processes has been documented *in situ* for an Al-Cu alloy<sup>29,30</sup> while a separate study utilising

this ultra fast set-up measured the microstructural evolution of a copper powder during sintering.<sup>31</sup> The first experiments performed *in situ*, in a corrosive aqueous environment were performed by Marrow *et al.*<sup>32,33</sup> In the present work, observations of intergranular corrosion (IGC) and stress corrosion cracking propagation in aluminium alloy 5083 and 302 stainless steel were obtained from proof of concept experiments.

As indicated in the work referenced above, the microtomography technique has been shown to provide quantitative differences between what can be derived or speculated from surface observations compared with what is actually happening in the bulk of the material.<sup>4,15-18</sup> To the corrosion scientist it is of crucial importance to understand what occurs within the bulk of a material that is exposed to an aggressive aqueous environment. In many cases the majority of activity is below the visible surface. Moreover, analysis of a localised corrosion or environmentally assisted cracking event and determination of how the event interacts with the local microstructure within a volume in real time would be most advantageous.

Most observations of localised corrosion have been obtained through activity occurring on the surface of the material or in traditional, 2D post-mortem, destructive analysis (i.e. metallography) of cross-sections of the specimen. Traditional 2D visualisation techniques cannot resolve the complex geometries of localised corrosion sites and cracking as well as their interaction with the existing microstructure. Sites that appear to be separated in 2D analysis could in fact be connected in 3D analysis. Polishing can also induce considerable artefacts on the surface and possible distort observations and subsequent quantitative measurements. Extensive grain fallout when polishing IGC is a specific example of this. Moreover, these techniques could provide misleading evidence if not performed thoroughly and to completeness. This is the case in studies of transitions from pits to cracks in many systems. There remains much debate in the community concerning the need for localised corrosion sites for initiation of environmentally assisted cracking.

*In situ* examination provides the corrosion scientist with the ability to observe the evolution of localised corrosion and cracking within a single specimen. Traditionally, serial exposures and removals of multiple specimens have been used to develop an understanding of the stages involved in corrosion development and possible transitions to stress corrosion cracking.<sup>34</sup> Moreover, removal and reinsertion of a specimen from an aqueous environment for visual inspection is not recommended as changes in the localised chemistry can occur resulting in misleading corrosion morphologies and rates of attack.

In the present paper two continuing programmes, one investigating the IGC of an aluminium alloy and the other investigating the transition from pitting to stress corrosion cracking in steel, are presented to illustrate the power of the X-ray microtomography technique. The attractiveness of this technique to provide physical inputs and parameters useful in life prediction modelling and in efforts to understand the underlying mechanisms controlling localised corrosion and stress corrosion crack growth is evident.

## Experimental

The materials used in these studies were aluminium aerospace alloy AA2024 and 3Ni–Cr–Mo–V steam turbine disk steel for the synchrotron and microfocus tomography experiments respectively. Material composition and relevant heat treatments are given in Table 1. AA2024 was used in a sensitised temper for *ex situ* corrosion/tomography experiments while specific regions of a friction stir welded AA2024-T351 plate were used for the *in situ* corrosion/tomography experiments as described below. The sensitised AA2024 temper was previously shown to simulate the electrochemical behaviour of the heat affected zone (HAZ) in the friction stir welded plate.<sup>35</sup>

### Synchrotron X-ray microtomography

The high resolution imaging and resultant spatial resolution of the reconstructed data characteristic of synchrotron microtomography require small sample cross-sections on the order of approximately 0.25–2 mm<sup>2</sup>. Sample size is dictated by the need to balance X-ray scintillator efficiency, signal to noise ratio and levels of X-ray transmission/absorption contrast through the material. Typically the X-ray energy must be relatively low (e.g. 35 keV). At these low energies specimens must remain small to ensure sufficient transmission of the incident X-ray beam.

‘Matchstick’ specimens (see Fig. 1a) were produced by initially machining 3 mm diameter rods from the centre plane of 6 mm thick rolled plate and subsequently turning down the upper 2 mm of the rod to form a 500 µm diameter cylinder/pin. Lacquer was applied to ensure that only the 500 µm diameter pin was exposed to the corrosive environments. The axis of the rods was oriented perpendicular to the rolling direction of the original aluminium plate. Specimens were produced from the parent material, as well as the nugget and HAZ of the FSW. Precise machining was performed to ensure that the pin region of the ‘matchstick’ specimen contained the relevant microstructure/weld region.

*Ex situ* corrosion/X-ray tomographic experiments were performed at the European synchrotron radiation facility (ESRF) on the high resolution tomography beam line (ID19). X-ray tomography was performed using a parallel monochromatic beam with an energy of 20.5 keV. The distance between the detector (2048 × 2048 CCD camera) and the ‘matchstick’ specimen was 10 mm. A series of 900 2D radiographs were recorded by rotating each sample through 180° with a 0.3 s exposure/projection and a 0.2° rotation between each scan. Image slices of the cross-section of the specimen (i.e. tomographs) were reconstructed from the 2D radiographs via a filtered back projection algorithm<sup>36,37</sup> resulting in a theoretical isotropic voxel (i.e.

3D pixel) resolution of 0.7 µm. Image analysis, visualisation and 3D rendering were performed using a commercial software package (i.e. Amira). Further details of the high resolution tomography beam line at ESRF can be found elsewhere.<sup>38</sup> Sensitised AA2024 ‘matchstick’ specimens were corroded before the tomographic scans. Specimens were exposed for 1, 3 and 5 days to neutral and acidified (i.e. adjusted to pH 3 with acetic acid) 0.6M NaCl at room temperature under an open circuit condition. After the desired exposure time, specimens were rinsed in deionised water, hot air dried, and stored in a desiccated chamber until scanned at the synchrotron facility.

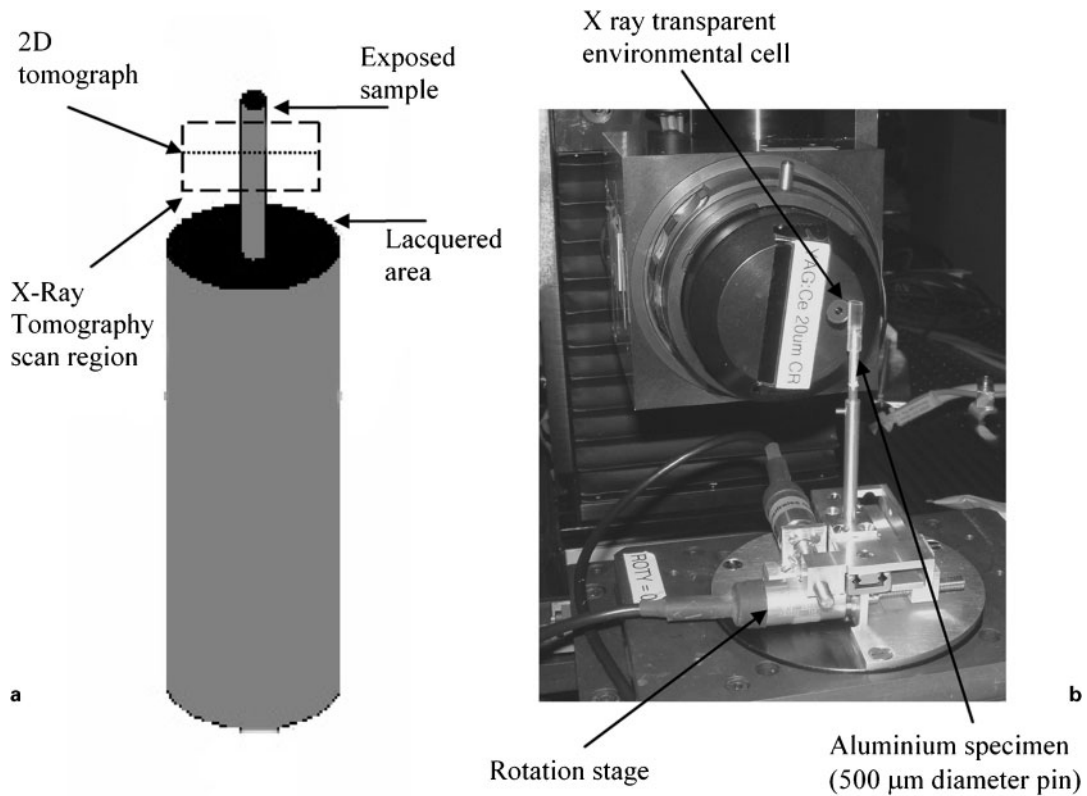
*In situ* corrosion/X-ray tomographic experiments were performed at the SLS on the materials science beam line (X04SA). Tomographic scans were performed on AA2024-T351 FSW specimens immersed in a corrosive environment over a period of 48 h. ‘Matchstick’ specimens of the parent region, HAZ and nugget region of the weld were exposed to 0.6M NaCl at room temperature at open circuit. A sequence of tomographic scans was performed on each specimen at ~5 h intervals during exposure. Scan times for each experiment were, on average, between 40 and 60 min in duration. For the *in situ* corrosion experiments on the beam line, a very simple environmental cell was constructed from ~3 mm internal diameter silicon rubber tubing (see Fig. 1b). The tubing was fitted around the base of the specimen rod and then filled with solution. Only the 500 µm diameter pin was exposed to the corrosive environment. Deionised water was added to the environmental cell when necessary owing to evaporation during the exposure time. During the *in situ* corrosion tests X-ray tomography was performed using a parallel monochromatic beam with an energy of 17.5 keV. A series of 1023 2D radiographs were recorded by rotating each sample through 180° utilising a 0.3 s exposure/projection. Image slices with a voxel resolution of 0.7 µm were reconstructed via a filtered back projection algorithm.<sup>36,37</sup> Image analysis, visualisation and 3D rendering were once again performed using a commercial software package (i.e. Amira). Further details of the tomographic beam line at SLS can be found elsewhere.<sup>39–41</sup>

### Microfocus computed X-ray tomography

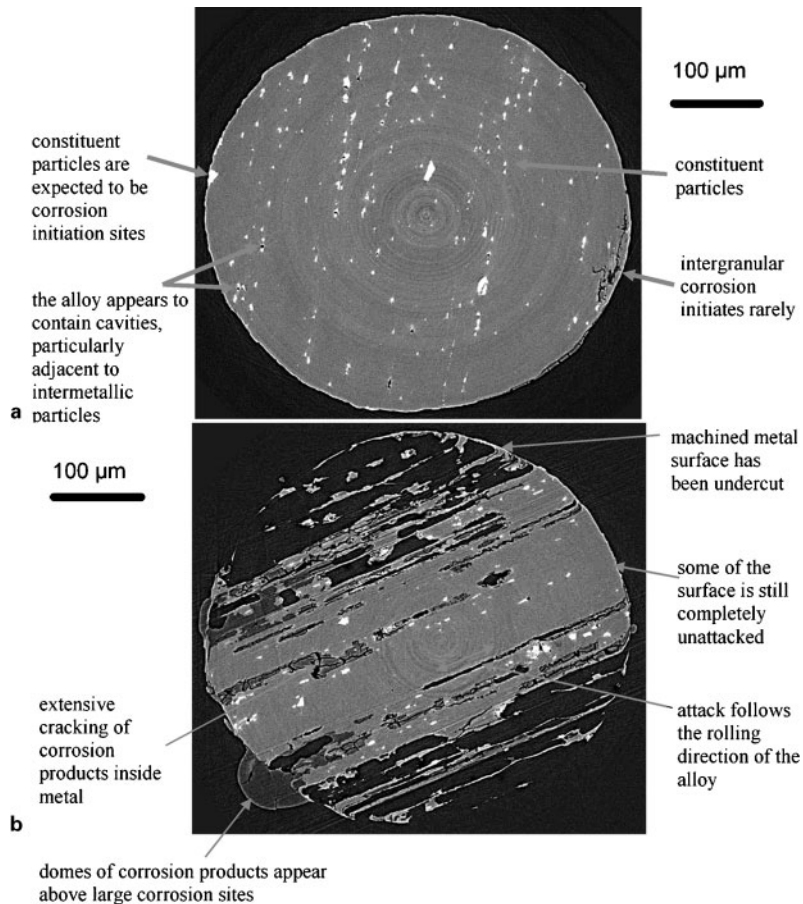
Microfocus X-ray tomography utilising a Skyscan 1072 high resolution desktop microCT system with an aluminium filter was used to characterise pitting and the transition to stress corrosion cracking in a 3Ni–Cr–Mo–V steam turbine disc steel. Scans were performed on specimens which had been previously<sup>42–47</sup> exposed to a simulated corrosive condensate environment (i.e. 1.5 ppm Cl<sup>-</sup> aqueous environment) at 90°C for up to 10 000 h while stressed at 90%  $\sigma_{ys}$ . The specimen shown in the present paper was exposed for 7173 h under these

**Table 1** Material compositions and relevant heat treatments

Material	Composition, wt-%	Relevant heat treatment/form
Aluminium aerospace alloy (AA2024)	4.6Cu–1.2Mg–0.6Mn–0.1Fe–0.1Si–0.06Cr–0.04Ti	Sensitised T8:T351 + 250°C for 2 h, water quench Friction stir weld (FSW): parent plate T351 FSW: weld HAZ FSW: weld nugget region
Steam turbine disk steel (3Ni–Cr–Mo–V)	Fe–2.89Ni–0.69Cr–0.45Mn–0.27Mo–0.28Si–0.091V–0.017P–0.013S–0.21N–0.3C	Stress relieved 625°C for 2 h



1 a schematic representation of 'matchstick' specimens used for *ex situ* and *in situ* corrosion studies on AA2024 (axis of 500 µm diameter cylinder was aligned perpendicular to plate's original rolling direction) and b photograph of *in situ* corrosion/X-ray tomography experimental set-up utilised at Swiss light source (SLS) revealing simple nature of X-ray transparent environmental cell



2 Reconstructed tomographic slice of single plane through cylindrical 'matchstick'/pin specimen of sensitised AA2024 (i.e. heat treated 250°C for 2 h) that has been exposed *ex situ* in 0.6M NaCl for a 24 and b 72 h under open circuit conditions at room temperature (data obtained ESRF ID19)

conditions. A quartered section, having an effective specimen thickness of 3 mm, of the original tensile bar gauge diameter was used to optimise X-ray transmission and resolution. Tomography was performed using a polychromatic divergent beam with a peak beam energy of 101 keV. A magnification of  $\times 70$  was selected resulting in a theoretical spatial resolution of 3.9  $\mu\text{m}$ . A series of 207 2D radiographs were recorded by rotating the specimen through  $180^\circ$  with an 11 s exposure/projection and a  $0.9^\circ$  step interval. Cross-section images of the specimen were reconstructed via a modified Feldkamp cone beam volumetric reconstruction algorithm creating a 3D representation of the internal corrosion and cracking features.<sup>37</sup> Image analysis, visualisation and 3D rendering were once again performed using commercial software packages (i.e. Amira, TView and CTVOL).

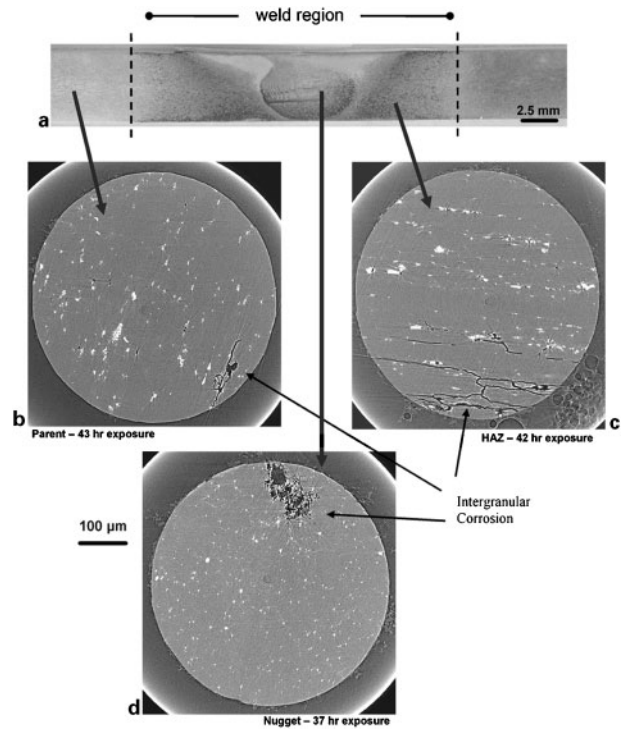
## Results and discussion

### Synchrotron X-ray microtomography

As part of an continuing programme investigating the localised corrosion behaviour of aluminium FSWs, *ex situ* and *in situ* synchrotron X-ray microtomography experiments have been used to visualise the morphology and quantify the rate of localised corrosion, specifically IGC, occurring within the bulk of the material. One of the concerns in using this solid state welding process in structural material is the enhanced susceptibility of the weld region to localised corrosion. The varied microstructure produced by the welding process provides an interesting system to study the evolution of corrosion morphology as a function of the differing microstructure associated with various regions of the weld.

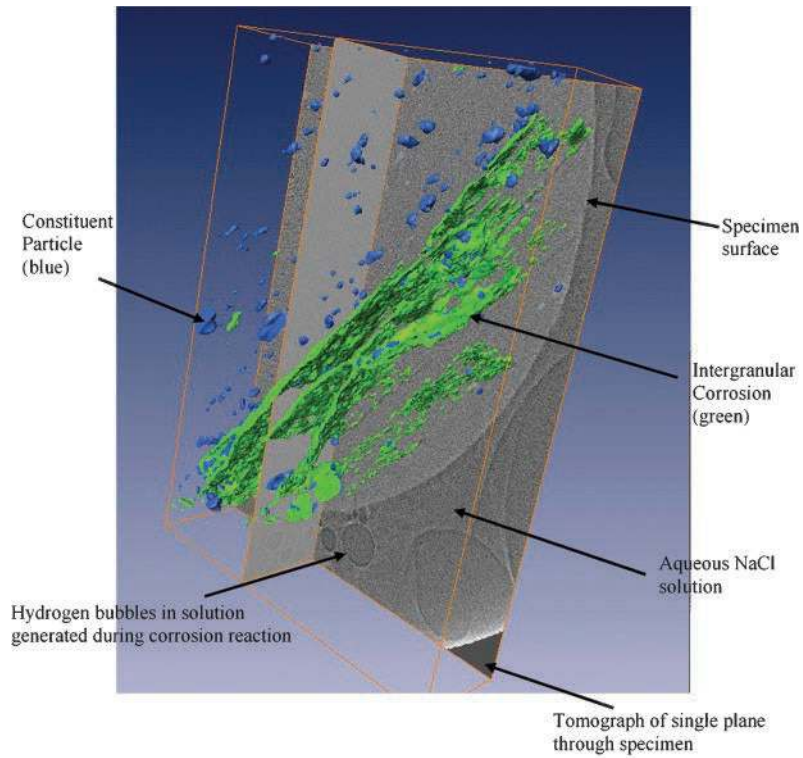
Intergranular corrosion in aluminium alloys, in general, is a problem of fundamental interest to the corrosion community, and is poorly understood. Accurate IGC rates are difficult if not impossible to quantify using conventional 2D measuring methods. Of particular interest in the determination of how IGC propagates from localised corrosion sites such as pits associated with large (i.e. 3–10  $\mu\text{m}$ ) intermetallic particles in the alloy. Furthermore, it is important to assess how the presence of these intermetallic particles affects the propagation of intergranular attack. This aspect of IGC is nearly impossible to study by 2D cross-sectional analysis as the probability of visualising the tip of an intergranular attack front interacting with an intermetallic particle is extremely low. Moreover, when using destructive 2D techniques, there is no opportunity to assess the time dependent nature of the corrosive attack.

Proof of concept experiments to determine the capability of synchrotron X-ray tomography for visualisation of corrosion in aluminium alloys were performed on sensitised AA2024 ‘matchstick’ specimens that were exposed *ex situ* in chloride solution. Figure 2a and b shows examples of two reconstructed tomographic slices, after 1 and 3 days exposures respectively, of single planes within the bulk of the cylindrical specimens. Differences in the X-ray absorption coefficients, which are seen as differences in contrast in the tomographs, of objects within the bulk of the specimen provide for good visualisation. Features in Fig. 2a such as high atomic number containing constituent particles which appear in bands along the rolling direction of the alloy plate,

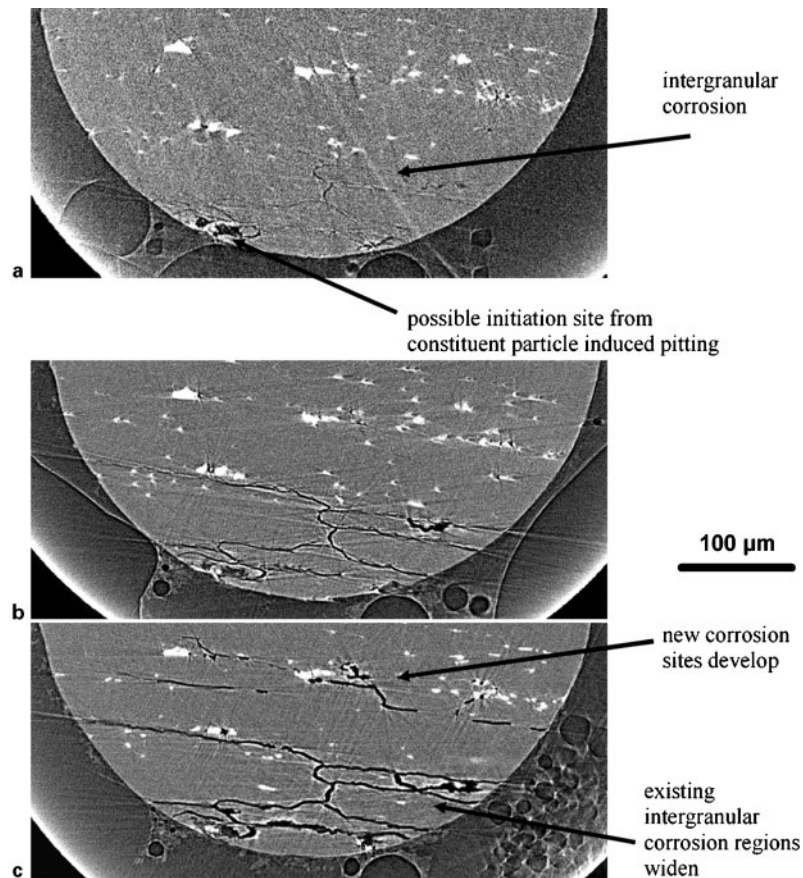


**3 a typical morphology of AA2024-T351 FSW after immersion in acidified sodium chloride environment for 24 h (ASTM G110 IGC susceptibility test) and reconstructed tomographic slices of single planes through cylindrical ‘matchstick’ specimens exposed *in situ* to 0.6M NaCl illustrating differences in IGC morphology as function of weld region for b parent plate, c weld HAZ and d weld nugget: differences in susceptibility are evident for three regions of weld; note that hydrogen bubbles from supporting cathodic reactions on specimen are evident in each tomography in aqueous solution within environmental test cell (data obtained SLS X04SA)**

porosity or cavities beside these constituent particles which form during the rolling process and IGC owing to exposure to the corrosive environment are easily defined and quantified. Two things should be noted concerning the corrosion morphology displayed after the 1 day exposure. First, it is clearly evident from Fig. 2a that, initially, IGC initiates rarely within the microstructure. Second, localised corrosion initiation does not readily occur at all constituent particles that are exposed to the corrosive environment. Figure 2b shows the extent of corrosion in the specimen after 3 days exposure in NaCl solution. Extensive amounts of IGC with a considerable amount of grain interior dissolution and/or fallout is evident. It should be remembered that these tomographic experiments were performed *ex situ* and consequently corrosion product can also be visualised. In the tomographs, the corrosion product has a slightly darker contrast compared with the matrix of the alloy. Large domes of corrosion product are visible on the surface of the specimen while solid and cracked corrosion product is visible within the IGC sites. One last observation should be noted from Fig. 2b. There appears to be an area on the surface of the specimen where the corrosion rate is lower than the bulk of the material and results in considerable undercutting. This may be an indication that the machining performed to manufacture the



4 3D rendering of multiple (i.e. on order of 200) tomographic slices containing tomograph displayed in Fig. 3c: only IGC and constituent particles have been visualised in 3D; IGC in 200 slices has been labelled as green while constituent particles have been labelled as blue (data obtained SLS X04SA); colours refer to online version only



5 Reconstructed X-ray tomographs of same, single plane through AA2024 FSW HAZ 'matchstick' specimen after exposure *in situ* in 0.6M NaCl after *a* 5, *b* 20 and *c* 42 h: morphology and extent of propagating IGC as function of time are well documented (data obtained by SLS X04SA)

'matchstick' specimens has an effect on the corrosion susceptibility and rate of attack local to the surface.

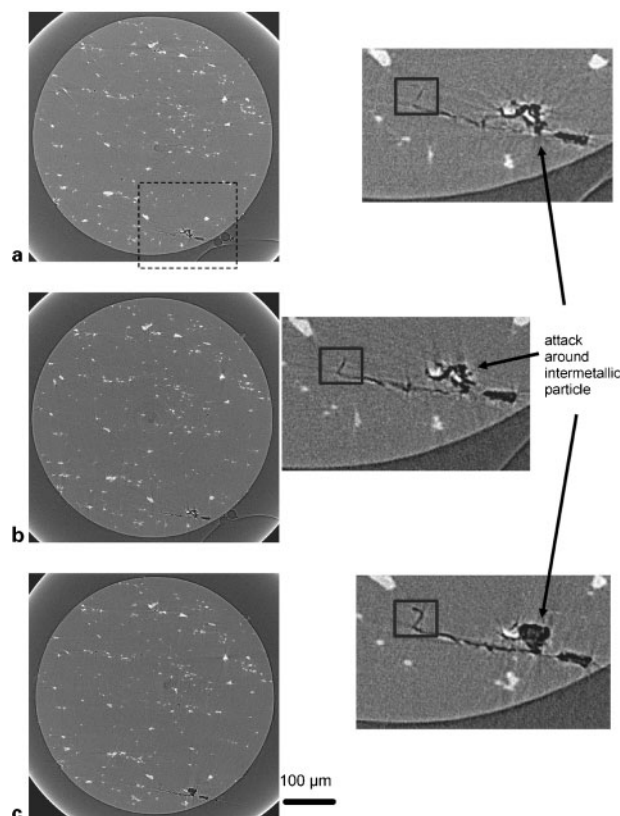
The propagation of IGC through AA2024 FSWs as a function of time and position in the weld has been studied via *in situ* tomographic scans carried out on individual specimens at 4–8 different times during continuous exposure. These experiments show the progressive development and coalescence of localised corrosion sites within the bulk of the sample and quantify the mode and rate of intergranular attack for the different microstructural regions of the weld.

Figure 3 displays the differing IGC morphology as a function of position across the FSW. Typical corrosion morphology of an AA2024-T351 FSW after immersion in an acidified sodium chloride environment (ASTM G110) is shown in Fig. 3a. Preferential localised corrosion attack, indicated by discoloration, is evident within the nugget and HAZ of the weld. Figure 3b–d presents tomographic slices of single planes within specimens of the parent plate, HAZ and nugget region of the weld respectively, after exposure in 0.6M NaCl for ~40 h. Each tomograph displays different morphology and extent of IGC as a function of weld position. The differing IGC morphology in the nugget region of the weld compared with that of the parent and HAZ reflects the change in microstructure owing to the welding process.

The information provided on each tomograph, such as that shown in Fig. 3c, can be combined spatially in a stack to provide a 3D representation of the IGC and alloy microstructure. Figure 4 presents a 3D rendering of the tomographic data for ~200 slices. The alloy matrix has been removed to reveal the interaction between IGC (green) and constituent particles (blue). In the associated tomographs (e.g. Fig. 3c) the IGC is shown as black while the constituent particles are white. This contrast correlates to the differences in X-ray absorption coefficients.

The development of localised corrosion attack within the HAZ of the AA2024 weld is shown in Fig. 5 as a function of continuous exposure time in 0.6M NaCl. It should be noted from the orientation and distribution of the constituent particles, that Fig. 5a–c is partial tomographs that visualise the same plane within the specimen after 5, 20 and 42 h respectively, of exposure in the aqueous chloride solution. Examination of the tomographic image after 5 h of exposure (Fig. 5a) reveals very slight indications of IGC emanating from a site on the surface of the cylindrical specimen. The site is possibly a constituent particle induced pit. The propagation of the IGC attack can be clearly seen in the subsequent tomographs (Fig. 5b and c). Note that not only is new IGC attack observed but that the existing IGC sites have also broadened in width.

The time dependent tomographic images in Fig. 6 record the interaction of a growing IGC site with a constituent particle within the bulk of a specimen. As the IGC propagates, one of the constituent particles appears to dissolve. Although the constituent particles generally support the cathodic reactions in the localised corrosion event the mechanism for this possible dissolution remains unclear. Comparison of the IGC in Figs 6 and 5 provides an indication of the differing rates of attack in the parent plate versus the HAZ. It is evident that the



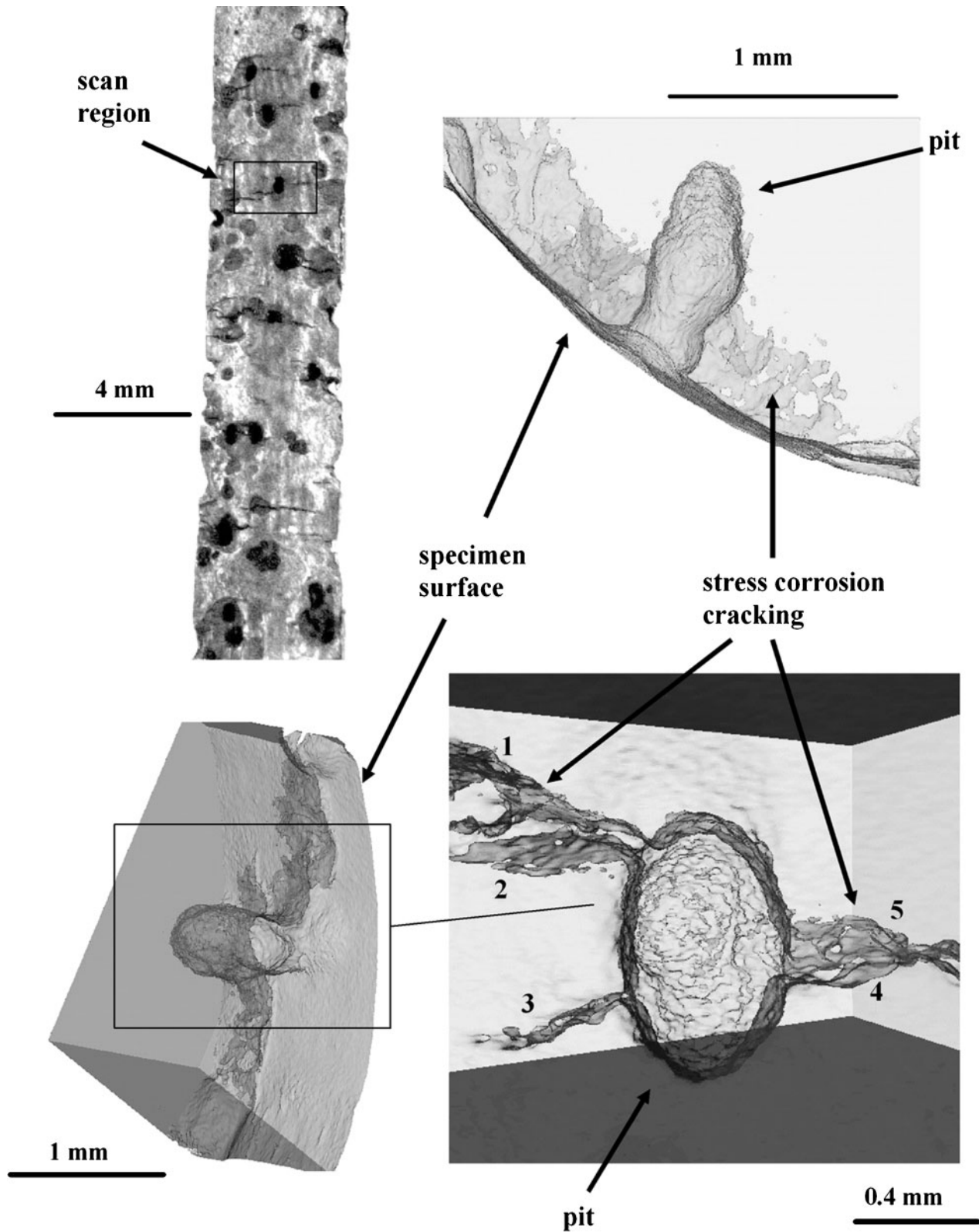
**6 Reconstructed X-ray tomographs of same, single plane through AA2024 FSW parent 'matchstick' specimen after exposure *in situ* in 0.6M NaCl after a 12, b 21 and c 31 h: series of tomographs illustrate interaction between region of propagating IGC and constituent particle (data obtained by SLS X04SA)**

kinetics of IGC within the HAZ is much greater than that found in the parent plate. Quantification of these IGC rates as a function of position across a FSW will be presented in a forthcoming publication.

### Microfocus computed X-ray tomography

As part of a larger programme<sup>42–47</sup> designed to provide a framework for predicting transitions from localised corrosion (i.e. pitting) to stress corrosion cracking of turbine disk steels, *ex situ* microfocus tube X-ray tomography experiments have been used to obtain 3D statistical detail of the distribution of pit size and cracks from long term test specimens previously exposed<sup>45</sup> in a simulated steam condensate environment. The acquired data will then be used in conjunction with data acquired utilising a destructive layer removal visualisation method<sup>47</sup> as input parameters to refine a developing model<sup>45,46</sup> to simulate the evolution of stress corrosion cracks from pits and therefore improve the predictive capability in service.

The power generation industry has experienced failures of steam turbine discs, rotors and blades owing to stress corrosion cracking which was often initiated from localised corrosion (i.e. pits). Stress corrosion cracking has been most often observed on low pressure turbines, where condensate films form typically at 90°C.<sup>43</sup> There is little information on the growth rate of pits, the initiation of cracks and subsequent crack growth in this system.



7 3D rendering of *ex situ* focus tube X-ray tomography experiment to visualise stress corrosion cracks emanating from large pits in 3Ni–Cr–Mo–V steam turbine disk steel tensile specimen that has undergone long term exposure stressed at 90% of  $\sigma_{ys}$  in aerated 1.5 ppm chloride aqueous environment at 90°C for 7173 h (NPL specimen 47); data obtained Skyscan 1072 high resolution microfocus CT system

It is of fundamental importance to predict the evolution of stress corrosion cracking from localised corrosion sites to more readily evaluate remnant life of the components. It is desirable to produce models that predict the probability of a crack initiating from a pit of

specific size, shape and depth. The strategic significance of predicting lifetime has instigated an effort in model development based on deterministic equations based on statistical input parameters pertaining to localised corrosion and environmentally assisted cracking in the

short and long crack regime.<sup>45,48–50</sup> Most of these models are continuum based and do not provide details as to how sustained environmentally assisted cracking evolves from a localised corrosion site. One widely accepted phenomenological model developed by Kondo suggests that for a pit to transition to a crack a pit must exceed a given depth which provides a threshold stress intensity factor (mechanical driving force) for crack initiation and the growth rate of the crack must exceed that of the pit.<sup>48</sup>

Initial attempts of modelling the transition from pits to cracks in the turbine disk steel system produced excellent predictions of the distribution of pit depths and the percentage of pits that transform to cracks when only surface cracks were considered.<sup>45</sup> Conventional observations of pit depth and the presence of surface cracks did not agree with the probabilistic likelihood that cracks had initiated from the given distribution of pits if subsurface cracking and more specifically cracks that neither broke the surface of the specimen nor extend past the base of the pit was considered.

Figure 7b–d depicts an example of 3D rendering of cracking associated with the well developed pit indicated on the surface of the specimen shown in Fig. 7a. The cracks emanating from the pit do not have depths into the material greater than that of the pit. It is of utmost importance to determine whether short cracks like these can initiate from the side instead of the base of a growing pit. From previous visualisation utilising the layer removal method, it was observed that 50% of the observed cracks that had extended to the surface of the specimen had depths that were less than the depth of the associated pit.<sup>47</sup> Several of the cracks emanating from the pit in Fig. 7 do not breach the surface of the specimen. The crack labelled 2 in Fig. 7d does not breach the surface of the specimen and seems to initiate at the side of the propagating pit. These observations question the validation of Kondo's model<sup>48</sup> which is based on linear elastic fracture mechanics that defines the stress intensity level as a function of the depth of the pit as essentially the same as the stress intensity level of a crack with the same depth. If crack initiation is more prevalent from the side of the pit compared with the base of the pit, this assumption would be an oversimplification of the actual pit to crack transition. On going, *ex situ* tomography work will be performed to provide further data from earlier exposure times of the crack morphology associated with smaller, younger pits.

## Conclusions

X-ray tomography, whether on a microfocus device or using a synchrotron source, has been shown to be a powerful tool in visualising, at the micrometre and submicrometre scale, localised corrosion within the bulk of a material. *Ex situ* and *in situ* experiments have been shown to provide a wealth of knowledge into the evolving morphology of localised corrosion and cracking.

Continuing analysis of the work from the two programmes presented in the present paper will make a significant contribution to the effort to elucidate the controlling electrochemical/physical mechanisms dictating the development of localised corrosion sites, specifically, the propagation of IGC in aluminium alloys and the transition from pitting to stress corrosion cracking in steels. Clearly defining the evolution of the

localised corrosion morphology as well as quantifying its growth rate of FSW AA2024 will provide a valuable underpinning that will significantly contribute to the continuing modelling effort for life prediction of aircraft components while clearly defining geometries governing the transition from pitting to stress corrosion cracking in turbine disk steels will add to the continuing effort for life prediction in the power generation industry.

## Acknowledgements

The authors gratefully acknowledge the provision of beam time at the SLS on the materials science beam line and at the ESRF on beam line ID 19. The authors would also like to thank the National Physical Laboratory, EPSRC, the Royal Society through the USA Research Fellow Programme (grant No. 15523), BAE Systems and Airbus UK for continuing technical and financial support. Finally, special thanks to Mr John Lane for his delicate machining of the 'matchstick' specimens used in the synchrotron experiments.

## References

1. L. Grodzins: *Nucl. Instrum. Methods Phys. Res.*, 1983, **206**, (3), 541–545.
2. L. Salvo, P. Cloetens, E. Maire, S. Zabler, J. J. Blandin, J. Y. Buffiere, W. Ludwig, E. Boller, D. Bellet and C. Josserond: *Nucl. Instrum. Methods Phys. Res. B*, 2003, **200B**, 273–286.
3. S. R. Stock: *Int. Mater. Rev.*, 1999, **44**, 141–164.
4. E. Maire, J.-Y. Buffiere, L. Salvo, J. J. Blandin, W. Ludwig and J. M. Letang: *Adv. Eng. Mater.*, 2001, **3**, (8), 539–546.
5. B. P. Flannery, H. W. Deckman, W. G. Roberge and K. L. Damico: *Science*, 1987, **237**, 1439–1444.
6. A. Sasov and D. van Dyck: *J. Microsc.*, 1998, **191**, (2), 151–158.
7. J. Cazaux, D. Erre, D. Mouze, J. M. Patat, S. Rondot, A. Sasov, P. Trebbia and A. Zolfaghari: *J. Phys.*, 1993, **3**, 2099–2104.
8. V. Kaftandjian, G. Peix, D. Babot and F. Peyrin: *J. X-ray Sci. Technol.*, 1996, **6**, 94–106.
9. L. F. de Oliveira, R. T. Lopes, E. F. O. de Jesus and D. Braz: *Nucl. Instrum. Methods Phys. Res. A*, 2003, **505A**, 573–576.
10. O. B. Olurin, M. Arnold, C. Korner and R. F. Singer: *Mater. Sci. Eng. A*, 2002, **A328**, 334.
11. W. Ludwig, J.-Y. Buffiere, S. Savelli and P. Cloetens: *Acta Mater.*, 2003, **51**, 585–598.
12. T. Ohgaki, H. Toda, I. Sinclair, J.-Y. Buffiere, W. Ludwig, T. Kobayashi, M. Niinomi and T. Akahori: *Mater. Sci. Eng. A*, 2005, **A406**, 261–267.
13. L. Babout, P. M. Mummery, T. J. Marrow, A. Tzelepi and P. J. Withers: *Carbon*, 2005, **43**, 765–774.
14. L. Babout, T. J. Marrow, P. M. Mummery and P. J. Withers: *Scr. Mater.*, 2006, **54**, 829–834.
15. J.-Y. Buffiere, E. Maire, P. Cloetens, G. Lormand and R. Fougères: *Acta Mater.*, 1999, **47**, 1613–1625.
16. A. Guvenilir, T. M. Breunig, J. H. Kinney and S. R. Stock: *Acta Mater.*, 1997, **45**, 1977–1987.
17. A. Guvenilir and S. R. Stock: *Fatigue Fract. Eng. Mater. Struct.*, 1998, **21**, 439–450.
18. A. Guvenilir, T. M. Breunig, J. H. Kinney and S. R. Stock: *Philos. Trans. Roy. Soc.*, 1999, **357**, 2755–2775.
19. T. J. Marrow, J.-Y. Buffiere, P. J. Withers, G. Johnson and D. Engelberg: *Int. J. Fatigue*, 2004, **26**, 717–725.
20. E. Ferrie, J.-Y. Buffiere and W. Ludwig: *Int. J. Fatigue*, 2005, **27**, 1215–1220.
21. H. Toda, I. Sinclair, J.-Y. Buffiere, E. Maire, K. H. Khor, P. Gregson and T. Kobayashi: *Acta Mater.*, 2004, **52**, 1305–1317.
22. E. Ferrie, J.-Y. Buffiere, W. Ludwig, A. Gravoil and L. Edwards: *Acta Mater.*, 2006, **54**, 111–1122.
23. K. H. Khor, J.-Y. Buffiere, W. Ludwig and I. Sinclair: *Scr. Mater.*, 2006, **55**, 47–50.
24. T. Dillard, F. N'Guyen, E. Maire, L. Salvo, S. Forest, Y. Bienvenu, J.-D. Bartout, M. Croset, R. Dendievel and P. Cloetens: *Philos. Mag.*, 2005, **85**, (19), 2147–2175.

25. J. A. Elliott, A. H. Windle, J. R. Hobdell, G. Eeckhaut, R. J. Oldman, W. Ludwig, E. Boller, P. Cloetens and J. Baruchel: *J. Mater. Sci.*, 2002, **37**, 1547–1555.
26. J. J. Gammage, D. S. Wilkinson, J. D. Embury and E. Maire: *Philos. Mag.*, 2005, **85**, 3191–3206.
27. L. Babout, E. Maire and R. Fougères: *Acta Mater.*, 2004, **52**, 2475–2487.
28. J.-Y. Buffiere, H. Proudhon, E. Ferrie, W. Ludwig, E. Maire and P. Cloetens: *Nucl. Instrum. Methods Phys. Res. B*, 2005, **238B**, 75–82.
29. O. Ludwig, M. Di Michiel, L. Salvo, M. Suery and P. Falus: *Metall. Mater. Trans. A*, 2005, **36A**, (6), 1515–1523.
30. A. Prasad, H. Henein, E. Maire and C.-A. Gandin: *Metall. Mater. Trans. A*, 2006, **37A**, (1), 249–257.
31. M. Di Michiel, J. M. Merino, D. Fernandez-Carreiras, T. Buslaps, V. Honkimaki, P. Falus, T. Martins and O. Svensson: *Rev. Sci. Instrum.*, 2005, **76**, 043702.
32. T. J. Marrow, L. Babout, B. J. Connolly, D. Engelberg, G. Johnson, J.-Y. Buffiere, P. J. Withers and R. C. Newman: in 'Environmentally induced cracking of materials II', (ed. S. Shipilov), 2006, Oxford, Elsevier Science.
33. T. J. Marrow, L. Babout, A. P. Jivkov, P. Wood, D. Engelberg, N. Stevens, P. J. Withers and R. C. Newman: *J. Nucl. Mater.*, 2006, **352**, (1–3), 62–74.
34. B. J. Connolly and J. R. Scully: *Corrosion*, 2005, **61**, (12), 1145–1166.
35. M. Jariyaboon, A. J. Davenport, R. Ambat, B. J. Connolly, S. W. Williams and D. A. Price: *Corros. Sci.*, 2006, to be published.
36. G. T. Herman: 'Image reconstruction from projections: the fundamentals of computerised tomography'; 1980, New York, Academic.
37. L. A. Feldkamp, L. C. Davis and J. W. Kress: *J. Opt. Soc.*, 1984, **1**, (6), 612.
38. W. Ludwig, J.-Y. Buffiere, S. Savelli and P. Cloetens: *Acta Mater.*, 2003, **51**, 585–589.
39. B. D. Patterson, C. Bronnimann, D. Maden, F. Gozzo, A. Groso, B. Schmitt, M. Stampanoni and P. R. Willmott: *Nucl. Instrum. Methods Phys. Res. A*, 2005, **540A**, (1), 42–67.
40. M. Stampanoni, G. L. Borchert, R. Abela, B. Patterson, D. Vermeulen, P. Ruegsegger and P. Wyss: *Acta Phys. Polonica B*, 2002, **33B**, (1), 463–469.
41. M. Stampanoni, G. Borchert, P. Wyss, R. Abela, B. Patterson, S. Hunt, D. Vermeulen and P. Ruegsegger: *Nucl. Instrum. Methods Phys. Res. A*, 2002, **491A**, (1–2), 291–301.
42. S. Zhou and A. Turnbull: *Corros. Eng. Sci. Technol.*, 2003, **38**, (2), 97–111.
43. A. Turnbull and S. Zhou: *Corros. Eng. Sci. Technol.*, 2003, **38**, (3), 177–191.
44. A. Turnbull, S. Zhou and G. Hinds: *Corros. Sci.*, 2004, **46**, 193–211.
45. A. Turnbull and S. Zhou: *Corros. Sci.*, 2004, **46**, 1239–1264.
46. A. Turnbull, L. N. McCartney and S. Zhou: *Scr. Mater.*, 2006, **54**, 575–578.
47. A. Turnbull, S. Zhou, L. Orkney and N. McCormick: *Corros. Sci.*, 2006, **48**, 2084–2105.
48. Y. Kondo: *Corrosion*, 1989, **45**, 7–11.
49. R. P. Wei: in 'Environmentally assisted cracking: predictive methods for risk assessment and evaluation of material, equipment and structures', (ed. R. D. Kane), 3–19; 2000, West Conshohocken, PA, ASTM STP 1401.
50. G. Engelhardt and D. D. Macdonald: *Corros. Sci.*, 2004, **46**, 2755.